ACS APPLIED MATERIALS & INTERFACES

Research Article

www.acsami.org

Direct Measurement of Chemical Distributions in Heterogeneous Coatings

Kayla A. Cooley,[†] Thomas P. Pearl,[†] Mark J. Varady,[†] Brent A. Mantooth,[‡] and Matthew P. Willis*[,‡]

[†]OptiMetrics, Inc. a DCS Company, 100 Walter Ward Boulevard, Suite 100, Abingdon, Maryland 21009, United States

[‡]Decontamination Sciences Branch, U.S. Army Edgewood Chemical Biological Center, 5183 Blackhawk Road, Aberdeen Proving Ground, Maryland 21010-5424, United States

Supporting Information

ABSTRACT: Chemical warfare agents (CWA) can be absorbed by variety of materials including polymeric coatings like paints through bulk liquid contact, thus presenting touch and vapor hazards to interacting personnel. In order for accurate hazard assessments and subsequent decontamination approaches to be designed, it is necessary to characterize the absorption and distribution of highly toxic species, as well as their chemical simulant analogs, in the subsurface of engineered, heterogeneous materials. Using a combination of judicious sample preparation in concert with scanning electron microscopy (SEM) and energy dispersive spectroscopy (EDS), it should be possible to directly measure the uptake and distribution of CWA simulants in the subsurface of complex multilayer coatings. Polyurethane and alkyd coatings were applied to aluminum and silicon substrates and contaminated with 2-chloroethyl ethyl sulfide (CEES) and dimethyl methylphosphonate (DMMP). The surfaces and cross-sectional interfaces of the contaminated coatings were probed with SEM-EDS to provide imaging, spectral, and elemental mapping data of the contaminant-material systems. This work demonstrated SEM-EDS capability to detect and spatially resolve unique elemental signatures of CWA simulants within military coatings. The visual and quantitative results provided by these direct measurements illustrate contaminant spatial distributions, provide order-of-magnitude approximations for diffusion coefficients, and reveal material characteristics that may impact contaminant transport into complex coating materials. It was found that contaminant uptake was significantly different between the topcoat and primer layers.

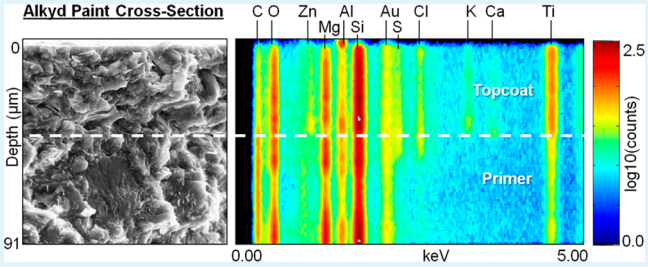

KEYWORDS: *SEM, EDS, CEES, DMMP, military coatings, molecular absorption, chemical distribution*

INTRODUCTION

Widespread use and applications of coatings demand constant improvement and examination of behaviors and performance as a function of environment. An important issue to consider in the function of protective coatings and films is resistance to absorption or permeation of chemical species. Subsurface measurements, particularly chemical and concentration depth profiles of coatings and their cross sections are of importance for materials science and biomedical applications, where chemical species penetration may seriously affect material integrity and performance.[1−3]

A variety of different spectroscopic techniques have been utilized for measuring absorption in permeable materials. Polymer films and coatings have been examined by confocal Raman microscopy to produce noninvasive depth profiles.[4] Fourier transform infrared photoacoustic (FTIR-PAS) and attenuated total reflectance (FTIR-ATR) spectroscopies have been implemented in the study of molecular transport into a single layer polymer as well as subsurface measurements and three-dimensional chemical imaging of thin, multilayered polymeric coatings.[5−7] Furthermore, FTIR has been used in conjunction with scanning electron microscopy (SEM) and energy dispersive spectroscopy (EDS) to characterize changes in the chemical distribution and composition of coatings throughout the service life of automotive components.[8]

SEM is a well-established materials characterization tool, commonly used to investigate topographical features in coatings production and to assess material performance. When coupled with EDS, SEM also permits examination of elemental composition and spatial distributions of material surfaces and cross sections. These capabilities have been employed in a variety of coatings studies from characterization of paints and their degradation products to metal diffusion into a mesoporous thin film of metal oxide nanoparticles.[9,10]

Past work has shown that absorption of chemical warfare agent (CWA) molecules and their simulants occurs in paint coatings, including those used for military assets.[11,12] Absorption of toxic chemicals into coatings systems presents exposure risks to personnel interacting with these materials and creates systems that are challenging to decontaminate.

Received: July 9, 2014
Accepted: August 22, 2014
Published: August 22, 2014

Chemical warfare agent contamination of military coatings has not been directly characterized using common spectroscopic techniques. Knowledge of the spatial distribution of contaminant in a material is particularly significant to CWA decontamination studies, but direct measurement of molecular absorption and the resulting subsurface concentration profile can be difficult to achieve. Visualizing and quantifying contaminant penetration would offer direct observation of contaminant transport into multilayer coatings for a more thorough understanding of transport and associated mechanisms in the contaminant-material system and may, in return, inform improved decontamination methodologies. In the current study, three coatings systems including two polyurethane formulations and an alkyd paint coating were contaminated and examined by surface and cross-sectional SEM-EDS to study molecular absorption of the CWA simulants 2-chloroethyl ethyl sulfide (CEES) and dimethyl methylphosphonate (DMMP). CEES and DMMP were chosen on the basis of structural and chemical similarities to specific CWA, namely distilled mustard (HD) and the nerve agent VX, respectively. Previous work has indicated that CWA transport in materials is contaminant-material pair specific thus requiring the need for specific simulants to properly emulate specific agent type mass transport behavior.[12] These contaminant-material combinations involving simulants and military paint systems were used to demonstrate the ability of SEM-EDS to characterize the spatial distribution of these chemicals in these heterogeneous coating systems.

EXPERIMENTAL SECTION

Equipment. SEM and EDS experiments were performed with an Evex Mini-SEM SX3000. The instrument operates under high vacuum at electron accelerating voltages of 1−30 kV to enable high-resolution imaging at magnifications up to 30000× with a resolution limit of 8 nm. The SEM includes a light element X-ray detector with a beryllium ultrathin window for EDS studies. EDS spectral resolution is relatively high at 0.128 keV, a value set by the full width half-maximum of the Mn peak located at 5.894 keV. The SEM also provides a sample stage that cools specimens to temperatures reaching −52 °C. Lowering the sample temperature minimizes the buildup of surface-localized electrostatic charge to combat common negative imaging effects (e.g., image drift, noise) and facilitates analysis of nonconductive samples. Furthermore, the reduced temperature ensured that molecular transport was quenched at the appropriate chemical-material interaction residence time, given CEES and DMMP freezing points of −48.7 and −50 °C, respectively. For this work, the instrument was reconfigured so that the sample chamber and vacuum system are located within a chemical fume hood to allow for safe examination of highly toxic chemicals on the materials of interest, while the control electronics are located outside of the hood.

Materials. Samples were prepared at the Army Research Laboratory (ARL) at Aberdeen Proving Ground (APG). Air Force Advanced Performance Coating (APC), water-dispersible chemical agent resistant coating (CARC), and Navy ship coat samples were produced according to MIL-PRF-85285E, MIL-DTL-64159B, and MIL-PRF-24635E, respectively. The coatings specifications cite a nominal thickness of 100 μm that includes both topcoat and primer layers. Air Force APC samples contained an aliphatic and polyester polyurethane topcoat (50.5 ± 7.5 μm) and a chromated primer (19 ± 4 μm), both sprayed in accordance with ASTM D823 Method D and air-dried at least 14 days before testing. The water-dispersible CARC system includes a polyurethane topcoat (50 ± 5 μm), applied according to MIL-DTL-53072C standards, and a white epoxy primer coating (37.5 ± 5 μm), meeting MIL-DTL-53030 standards. The Navy coating samples were composed of a silicone alkyd topcoat (50.5 ± 7.5 μm) and a zinc molybdate primer (85.75 ± 12.25 μm), prepared following ASTM D823 and TT-P-645 standards, respectively. These specifications set quality standards for coating generally large military assets, where slight, localized differences in coating or layer thicknesses and/or composition are negligible relative to the size or surface area of the asset. Although SEM and EDS material studies revealed generally uniform material characteristics within a military coating type, some intra- and intersample variations in thickness and composition were evident. Samples used in this study were chosen with similar total thicknesses across all three coating types for each contamination time. Due to the heterogeneity of the materials, variations in material composition at the micron measurement length scale appear within data analysis of contamination.

To meet SEM chamber size requirements and to enable SEM-EDS analysis, the coatings were applied to 12.5 mm diameter aluminum pin stubs (Ted Pella, Standard Pin Stub Mount) and 20 mm × 20 mm silicon fragments (Ted Pella, *p*-type Si(100)) for surface and cross-sectional examination. Coating aluminum pin stubs provided clean, smooth, and SEM-ready samples for surface contamination analysis and using silicon wafer substrates enabled coatings to be cleaved along a silicon crystal plane to reveal cross-sectional interfaces of the contaminated coatings. Other methods like cutting the coatings with a razor or more conventional cross-sectioning techniques such as focused ion beam milling and microtomy would be unsuitable to study these materials. Each of these methods would likely cause widespread material redistribution and/or mechanical stresses that would affect contaminant distribution within the material. SEM-EDS examination has demonstrated that the cleaved samples provide well-defined cross-sectional interfaces with minimal material redistribution (e.g., no material shearing).

Chemicals. Paint samples were dosed with CEES (98%, Sigma Aldrich, 693-07-2) and DMMP (97%, Sigma Aldrich, 756-79-6) to simulate HD and VX contamination, respectively. Air Force and Navy samples were contaminated with a single 20 μL drop of liquid simulant delivered by a positive displacement pipette with the sample surface oriented horizontally. Initial experiments with water-dispersible CARC demonstrated that 20 μL drops spread across the material surface and were quickly absorbed by the coating (as seen in the Supporting Information, Figure S1), so further experiments used 40 μL drops in order to maintain a high enough contaminant concentration at the center of the substrate (approximate location for SEM measurement). The volume of liquid was chosen such that there was visible bulk liquid on the sample surface during the entire contamination time. Contaminated samples were covered with a glass Petri dish and allowed to sit at room temperature in a chemical fume hood for either 5 or 30 min in order to capture the system with different concentration distributions en route to saturation. After the contaminant residence period, any excess liquid contaminant was wicked away from the sample surface using a Kimwipe. The degree of droplet spreading, evaporation, and sorption into the samples varied as a function of contaminant and paint coating.

Measurements. Contaminated samples were subjected to both surface and cross-sectional examination to study the mass transport behavior of CWA simulants into the coatings as a function of sample composition and structure. Sample preparation for cross-sectional examination involved one additional step of cleaving the material to reveal the cross-sectional interface after contamination and aging. The backside of the silicon bases of the samples were scored with a diamond scribe before contamination, and after the appropriate contamination time, a quickly applied pressure, near the edge and away from the contamination site, induced cross-sectional cleavage. Because the coatings are nonconductive, all samples were sputter-coated with Au (∼10 nm thick) before introduction to the SEM chamber. Au was chosen as the conductive sputter coat because the primary EDS signal was unique from the signature contaminant and coating EDS signals. Although the introduction of a Au peak (2.120 keV) produced potential EDS peak overlap with P (2.013 keV), S (2.307 keV), or Cl (2.621 keV) signals, other common sputtering metals would have a similar overlap effect (e.g., Pt or Pd at 2.048 and 2.838 keV, respectively) or could enhance the coating signal provided by the paint formulation components (e.g., Cr flattening agents). Once

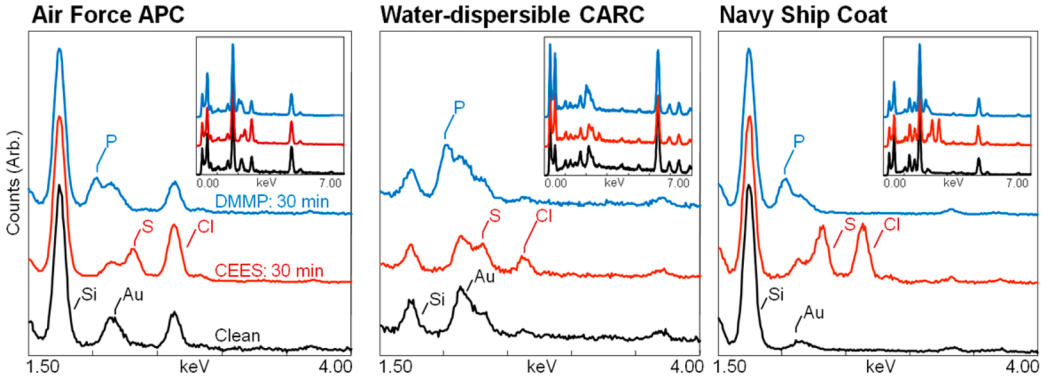

Figure 1. Surface EDS spectra of contaminated coatings. The EDS spectra represent clean samples (black) and samples contaminated with both CEES (red) and DMMP (blue) for 30 min. The S and Cl peaks at 2.307 and 2.621 keV, respectively, reveal CEES contamination, and the P peak at 2.013 keV indicates DMMP contamination. Other peaks along the region of interest include Si at 1.739 keV and Au at 2.120 keV. The insets provide wider energy range spectra for the surface of the coatings (topcoats).

low pressure was achieved, the sample was cooled from room temperature to −52 °C, a process taking 15−20 min. Approximately 30 min passed between the end of contamination and the start of measurements.

SEM-EDS spectra were collected using both top down and cleaved cross section perspectives. Using an accelerating voltage of 20 kV, SEM-EDS analysis of the material surface (top down view) involved collection of EDS spectra from 100 μm × 100 μm regions of the contaminated samples whereas the total analyzed cross-sectional areas were nominally 91 μm × 91 μm with some deviation due to variations in sample thickness. The spectra show the number of characteristic X-rays the material emitted over a 2 min collection time during which the electron beam continually raster scans the entire region of interest.

Elemental mapping of the sample cross sections was the primary analysis technique for providing paint layer specific EDS spectra and element specific depth profiles in the subsurface of the coatings. For cross sectional regions probed by EDS, a multispectral image was acquired. During EDS mapping acquisition the electron beam dwells for approximately 50 ms at each point (128 × 128 matrix of pixels) in the region of interest, during which X-ray spectra are recorded for each pixel.

Compilation of the spectra within the topcoat and primer layer regions allowed the layers to be analyzed for changes in elemental composition. Due to the proximity of P, Au, and S characteristic energies, Gaussian fits were necessary to deconvolve their overlapping EDS signals (as seen in the Supporting Information, Figure S2). This allowed integration of clearly defined P, S, and Cl peaks to calculate peak area for the contaminant signal at each contaminant residence time. Because the paint substrates were unpolished surfaces, irregular geometries could directly affect these intensity values, making comparison between samples potentially misleading. To normalize signals between samples, contaminant intensity values were divided by the intensity of an elemental signal that was constant within a material: titanium for Air Force APC layers, water-dispersible CARC primer, and Navy ship coat layers and chromium for water-dispersible CARC topcoat.

In addition to spectral data, Matlab (v. 2014a) routines were developed to calculate the average EDS intensity for elements as a function of depth in the sample (i.e., the average intensity for each horizontal row of the multispectral image is calculated for each X-ray energy) to allow for profile comparison across samples. While EDS signals spanning top down regions of a material produce constant material signals for normalization of contaminant peaks, normalization of one depth profile by another was inhibited by the heterogeneous distribution of paint components within the coatings cross sections. Thus, depth profiles present raw contaminant elemental signatures that were not normalized by a constant material signal. Time scale analysis of contamination penetration dynamics provided by the depth profiles allowed order-of-magnitude approximations of diffusion coefficients. The accuracy of diffusion coefficient approximations is primarily governed by EDS spatial resolution, determined to be <5 μm based on instrument settings and electron penetration depth.[13] Diffusivity estimates would tend toward overestimation given the lower spatial resolution of the elemental maps.

RESULTS AND DISCUSSION

Surface Analysis. Top down surface EDS analysis of all three coatings, shown in Figure 1, demonstrated SEM-EDS capability to detect CEES and DMMP contamination and supported subsurface measurements by providing an initial assessment for the elemental identification of contamination (see the Supporting Information, Figure S3 for surface EDS peak analysis). A unique elemental signature was required for differentiation of contaminant from the dosed material. As the materials of interest were polyurethane and alkyd coatings, the S and Cl Kα lines at 2.307 and 2.621 keV, respectively, in CEES-contaminated samples and the P Kα lines at 2.013 keV in DMMP-contaminated samples were optimal indicators of contamination.

EDS analysis presented in Figure 1 demonstrates the detectable increases in the S and Cl peak heights and elemental ratios after CEES contamination and increased P signals after DMMP contamination in all three materials. The baseline composition as determined by EDS of each paint system, as a function of layer type, was measured to account for precontamination abundances of S, Cl, and P. Both Air Force APC and water-dispersible CARC exhibited elemental overlaps that could complicate a clear delineation of the contaminant signal. For Air Force APC, the presence of Cl in the aliphatic polyurethane topcoat constrained EDS analysis of CEES contamination to the S signal, but the lack of phosphorus-rich particles enabled a more straightforward interpretation examination of DMMP contamination. Similarly, the clean water-dispersible CARC produced a weak S signal, making Cl the optimal signal to track CEES contamination in this material. Uncontaminated Navy ship coat did not contain any of the CEES or DMMP elemental markers, making all three elements prime candidates for tracking contamination in this material. Correlations between contaminant absorption and coating structure (see the Supporting Information, Figure S4) were made evident by the surface spectra. Although Air Force APC and Navy ship coat showed more notable increases in the Cl, S, and P signals after 30 min contamination times, the lower measured increases in contaminant signal at the surface of CARC can likely be attributed to rapid, capillary uptake, as

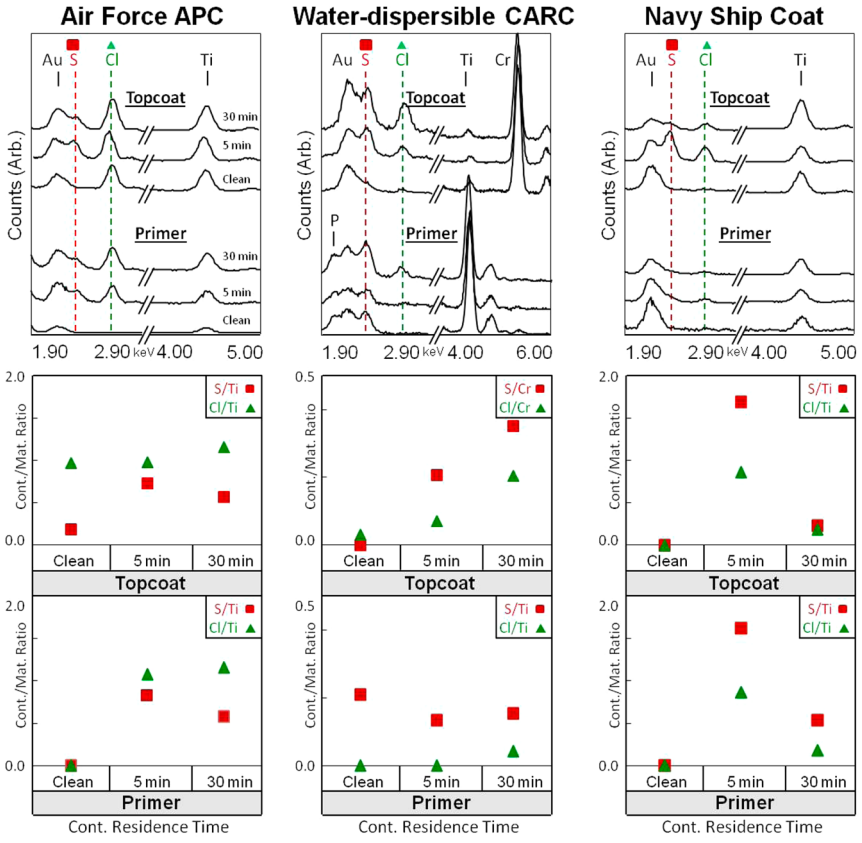

Figure 2. Cross-sectional EDS of military coatings comparing clean and CEES-contaminated conditions for both topcoat and primer layers. For uncontaminated samples, spectral analysis revealed the presence of Cl (2.621 keV) in the Air Force APC topcoat layer and the presence of S (2.307 keV) in the water-dispersible CARC primer layer. The spectra showed uncontaminated Navy ship coat to be free of S and Cl. The variability gauge charts used the ratio of deconvolved peak areas for select elements to reveal the evolution of the contaminant signal over time.

radial spreading of the liquid will cause the signal intensity at the center of the contaminated area to increase at a slower rate.

Cross-Sectional Analysis. EDS analysis of material cross sections enabled depth profiling of CEES and DMMP contamination and permitted visualization and quantification of contaminant distribution within the coatings. Figures 2 and 3 provide material composition data in the form of the sum spectrum of a region of interest from the cross-sectional image of all three military coatings for CEES and DMMP contaminated coatings. Variance in the material signals, particularly Ti and Cr, is due in part to intersample variance. These material signals serve as the best markers for relative abundance of contaminant to material elements as well as accounting for morphology effects on signals. The cross-sectional data from both Figures 2 and 3 reveal elemental differences between the topcoat and primer layers not readily apparent in the (top down) surface analysis in Figure 1. Further, the spectra show the evolution of the contaminant signal within the two paint layers at different contamination times. These results complement the depth profiles for CEES and DMMP contaminated coatings at 5 and 30 min contamination times located in Figure 4.

The cross-sectional EDS spectra in Figure 2 and Figure 3 showed the presence of Cl within Air Force APC topcoat and confirmed the material to be free of a possibly interfering S or P signal. For CEES contamination, the spectral data of the individual coating layers indicated contaminant presence within both paint layers, as evidenced by the appearance of a S peak in the topcoat and a Cl peak in the primer layer. Depth profiles shown in Figure 4 illustrate a contamination system where the strength of the contaminant signal increased slightly with droplet residence time on the material. The increase in intensity from the 5 to 30 min contamination time indicated that the topcoat was nearly but not fully saturated, although the contaminant was close to uniformly distributed spatially in the topcoat layer.

The observed penetration depths were used in a scaling analysis, shown in Table 1, to provide order-of-magnitude approximations of contaminant diffusion coefficients in each layer of the three coatings. The uniform distribution of contaminant in the topcoat indicates a lower limit on the diffusion coefficient in the topcoat, which can be estimated by $D \approx L^2/t_{cont}$, where L represents the topcoat layer thickness because the contaminant was detected throughout the layer. Diffusivity was estimated for primer layers as long as results in Figures 2 and 3 displayed an increase in contaminant signal and the depth profiles from Figure 4 indicated an elemental signature. Primer penetration depth estimations were limited to material within the 91 μm × 91 μm region of interest. For Air Force APC and water-dispersible CARC, the actual penetration depth may have exceeded the analyzed area, which would underestimate diffusivity approximations. Because contaminant molecules must transport through the topcoat, the primer signal is small and close to background. Contamination times, denoted by t_{cont}, included the contaminant residence period (5 or 30 min) and the time before measurements began (30 min) for totals of either 35 or 60 min. For the primer layer, t_{cont} uses the same values under the assumption that transport through

dx.doi.org/10.1021/am504487j | ACS Appl. Mater. Interfaces 2014, 6, 16289−16296

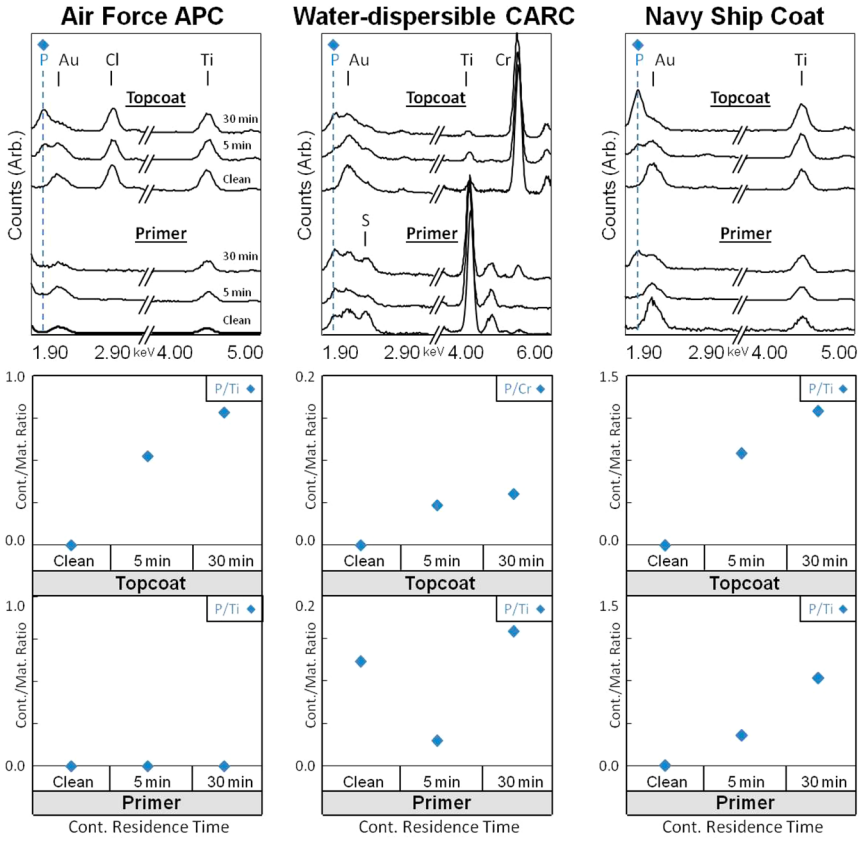

Figure 3. Cross-sectional EDS of military coatings comparing clean and DMMP-contaminated conditions for both topcoat and primer layers in each coating system. For uncontaminated samples, spectral analysis revealed the presence of P (2.013 keV) in the water-dispersible CARC primer layer and showed uncontaminated Air Force APC and Navy ship coat to be free of an interfering P signal. The variability gauge charts used the ratio of deconvolved peak areas for select elements to reveal the evolution of the contaminant signal over time.

the topcoat was less than 5 min as indicated by the uniform elemental distributions in Figure 4 at the 5 min residence time. The values produced by this analysis correspond to the magnitude of diffusion coefficients for heterogeneous polymeric materials.[14] Further, the difference in the magnitude of the contamination diffusion coefficient between two coating layers indicates a larger transport resistance in the primer layer.

DMMP contamination of Air Force APC behaved similarly to CEES contamination by absorbing into the entire topcoat layer; however, DMMP penetration into the primer layer was limited. The spectral and elemental mapping results suggest that the chromate primer was resistant to DMMP but not to CEES. The difference in molecular size and polarity between DMMP and CEES could be responsible for the chemical resistance. Furthermore, DMMP contamination of Air Force APC did not demonstrate a clear increase in contaminant signal intensity between 5 and 30 min contamination times. This uniformity could be the result of contaminant redistribution as a result of the time gap between contamination and measurement (~30 min) or a possible effect of the SEM vacuum environment on the contaminant-material system. Alternatively, the uniform contaminant depth profile could suggest that the transport resistance in the topcoat layer to be sufficiently low as to allow transport in the entire layer to be treated as a lumped capacitance system.

In addition to contamination depth profiling, elemental mapping revealed material influence on contaminant penetration. As demonstrated in Figure 5, each elemental map of contaminated Air Force APC exhibited circular voids within the contaminant distribution. These voids correspond to spherical particles contained in the topcoat layer, identified by EDS as carbon-rich polymeric flattening agents. While the polymeric beads do not show elemental evidence of contamination, the surrounding matrix, including the indentations where beads were once embedded, produced a strong contaminant signal. This marked behavior suggests that the contaminant is impeded by this material feature, indicating a heterogeneous contamination system where different coating components exhibit different transport resistances for the contaminant molecules.

As with surface analysis, elemental mapping of contaminated water-dispersible CARC was complicated by contaminant-material signal overlap. Although not clearly demonstrated by surface examination, the cross-sectional spectra showed water-dispersible CARC to contain S and P within the primer layer. The signal from these particles appeared very weak or negligible in Figure 1 due to the amount of material the X-rays from the primer coat had to traverse in order to reach the detector, as compared to the topcoat. Although not overwhelmingly intrusive in surface analysis, the effect of this contaminant-material signal overlap would be more significant in cross-sectional analysis, where the exposed primer coat would produce much stronger S and P signals. The cross-sectional spectra confirmed Cl to be the optimal signal to track CEES contamination in water-dispersible CARC and demonstrated that it may not be possible to clearly delineate the DMMP P signal from that of the primer in cross-sectional analysis of this material. The variability in S and P levels demonstrated in the cross-sectional time analysis of water-dispersible CARC primer

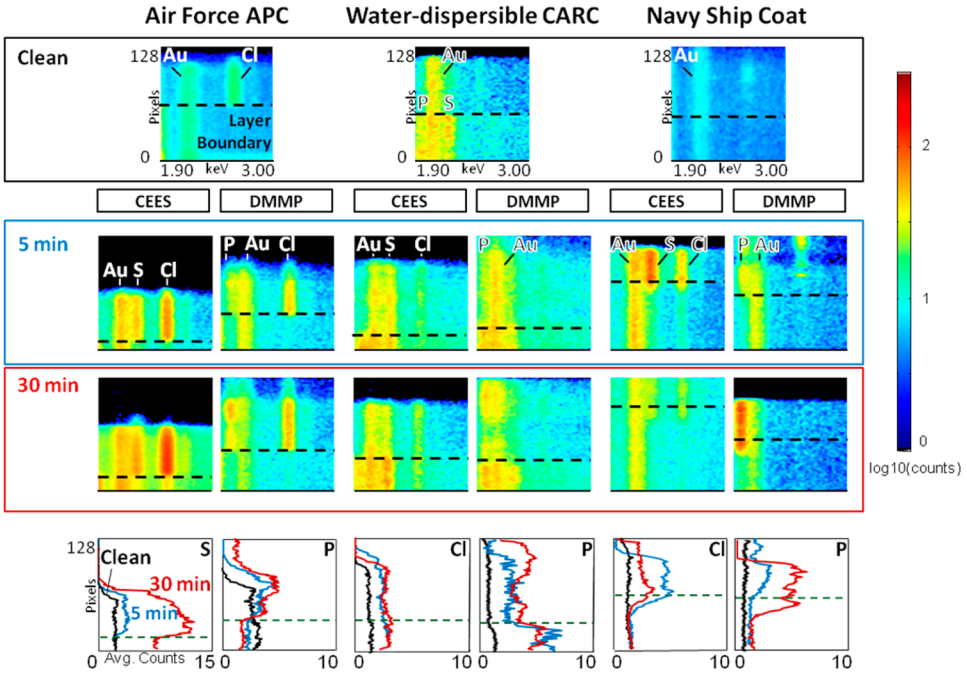

Figure 4. EDS depth profiles of uncontaminated and CEES and DMMP contaminated Air Force, CARC, and Navy coatings at 5 and 30 min contamination times. The multielement depth profiles (top three rows) reveal the penetration depth of elements with characteristic energies between 1.90 and 3.00 keV. CEES penetration is indicated by S (2.307 keV) and Cl (2.621 keV), and DMMP penetration is represented by P (2.013 keV). For the single element depth profiles (bottom row), S was used to track CEES contamination in Air Force whereas Cl was used in both CARC and Navy ship coat. DMMP was tracked with the P signal for all three materials. The dotted lines show the boundary between the topcoat and primer layers determined by elemental transitions specific to the topcoats and primer materials. All maps span a 91 μm × 91 μm area, excluding the fourth column, which represents 67 μm × 67 μm areas of CARC exposed to DMMP (a higher data collection magnification was used due to a lower coating thickness).

Table 1. Diffusion Coefficient Estimates for Simulants in Military Coatings

	D_{CEES} (m^2/s)		D_{DMMP} (m^2/s)	
coating	topcoat	primer	topcoat	primer
Air Force APC	6×10^{-13}	1×10^{-14}	2×10^{-13}	0[a]
Water-dispersible CARC	9×10^{-13}	9×10^{-14}	3×10^{-13}	0[a]
Navy ship coat	4×10^{-13}	3×10^{-14}	1×10^{-13}	2×10^{-14}

[a]No penetration observed.

can be most likely attributed to the heterogeneous distribution of the particles containing these elements, as opposed to contamination. This variability would likely cause overestimations of diffusivity approximations.

The cross-sectional EDS spectra show that the Cl signal in water-dispersible CARC topcoat increased after a 5 and 30 min exposure to CEES, and in both cases, the signal appeared to be uniformly distributed. Further, the spectra demonstrated penetration of the primer in the 30 min sample. It is likely that CARC's porous topcoat structure (as seen in the Supporting Information, Figure S2) facilitated fast capillary transport to the primer layer for a wider contaminant distribution than observed in the other military coatings.

For DMMP, contamination was not clearly discernible from the material in the elemental maps due to the presence of zinc phosphate in the primer coat. In spite of the signal overlap, EDS analysis showed an increase in the P signal strength as a result of contamination. The diffusivity magnitude approximation for the CARC primer was reported as negligible, because the phosphorus signal from DMMP could not be differentiated from zinc phosphate in the primer layer. While illuminating material-specific contaminant penetration and distribution characteristics, the CARC depth profiles establish the need to analyze contamination of individual paint layers to fully understand contaminant transport in this complex material.

Given the lack of contaminant-material overlap for Navy ship coat, Cl and P signals were used as signatures in the cross-sectional analyses for CEES and DMMP contamination, respectively. For both CEES and DMMP contamination, the contaminant signal was approximately uniform over the entire topcoat layer at both contamination times with very limited penetration into the primer layer. The EDS signal indicates that Cl and P penetrated approximately 10 μm into the primer which is greater than the EDS estimated resolution of 5 μm.[13] This could imply contaminant redistribution within the material between contaminant residence and SEM data collection. A number of the samples also demonstrated a distinct, strong intensity peak at the boundary between the two layers, which may indicate the possibility of contaminant accumulation at the interface between the primer and topcoat layers. In addition, there were gaps in the elemental maps within the nonporous topcoat, suggesting that the contaminant was impeded by certain impermeable particles in the polymeric matrix, illustrated in Figure 5.

Although DMMP contamination of Navy ship coat demonstrated a clear increase in contaminant signal strength from 5 to 30 min contamination times, 5 min exposure to CEES produced higher average intensities than a 30 min contamination time. This disparity could be the result of varied topcoat thicknesses; however, it is more likely the product of a

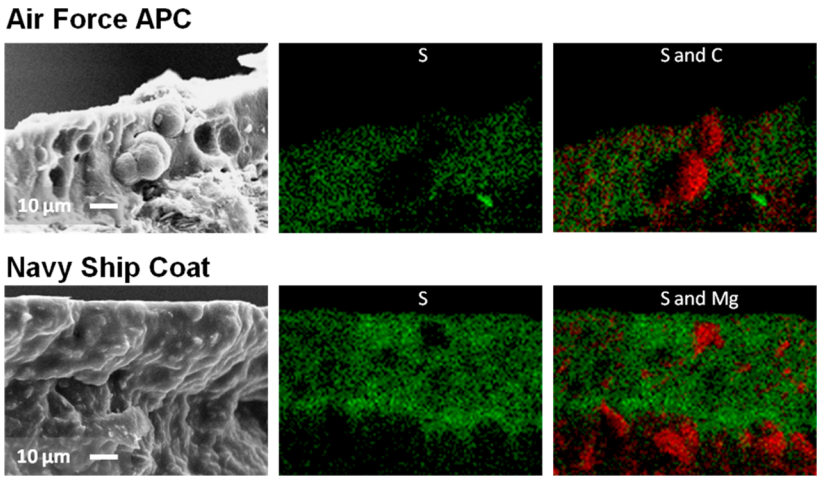

Figure 5. SEM and EDS mapping of CEES contaminated Air Force APC and Navy ship coat after a 30 min residence time. The middle two EDS maps demonstrate elemental distribution of S in the material cross-section in the matching SEM image. The top right map shows the presence of carbon-rich polymeric beads within Air Force APC topcoat and the bottom right map reveals the presence of magnesium-rich particles throughout Navy ship coat. These maps demonstrate the impermeability of the carbon-rich polymeric beads and the magnesium-rich particles in Air Force APC and Navy ship coat, respectively.

chemical reaction or dissolution mechanism between CEES and the coating. As opposed to the other two materials, which did not exhibit signs of a contaminant-material reaction, SEM revealed that exposure to CEES altered the surface morphology of Navy ship coat that interacted with the contaminant, making a pristine cross-sectional interface difficult to achieve after long exposure. For instance, a single cross section would demonstrate both well-defined and damaged areas as a result of cleaving. It is probable that the observed altering effect as a result of a 30 min contamination period allowed much of the contaminated area to soften so that areas near the center of the contamination area did not survive the cleaving process. As the damaged areas were unsuitable for EDS analysis, elemental mapping may not have clearly represented contamination of Navy ship coat after a 30 min contamination time. These results further demonstrate the need to study deconstructed coatings to better understand contamination of the entire coating system.

CONCLUSIONS

To meet the need of spatially resolved subsurface mass transport measurements in CWA decontamination studies, SEM-EDS was used to probe CEES and DMMP contamination of military coatings. Examination of the contaminated materials demonstrated the ability of SEM-EDS to resolve cross-sectional contamination at different contamination times, and EDS analysis established the capability to render depth profiles of contamination within coatings when there exists at least one elemental signature unique to the contaminant. Thus, these direct measurements provided visual and quantitative insight concerning contaminant distribution within multilayer, polymeric coatings.

Furthermore, SEM coupled with EDS has elucidated material characteristics that may affect contaminant transport into coating materials. Contamination of both Air Force APC and Navy ship coat by CEES and DMMP appeared to be largely isolated to the topcoat layer, regardless of contaminant residence time. This may be a direct effect of contrasting polymeric densities between the two layers, where a contaminant is able to move through the topcoat matrix more easily than the less permeable primer coat. Furthermore, widespread distribution of a contaminant in water-dispersible CARC is most likely aided by its porous topcoat allowing fast capillary transport to the primer layer. Second, there are regions of no contaminant signal in the contaminant elemental map corresponding to particles in the coating matrix of both Air Force APC and Navy ship coat. Thus, it is possible that these particles impede contaminant transport, thereby making contamination of these heterogeneous materials a complex system of spatially varying transport rates.

Further experimentation should focus on contamination of deconstructed coatings (e.g., polyurethane component of CARC without pigments, flattening particles) to understand how each major coating component influences contaminant molecular transport in the coating system and to assess possible material reactivity with the contaminant itself. Progress in these areas coupled with complementary research would provide pathways for the Chemical Biological Defense (CBD) community to further develop military coatings and to improve upon standard decontamination methods.

ASSOCIATED CONTENT

Supporting Information

Relevant experimental results and data not included in the paper associated with observations of contaminant liquid spreading on paint surfaces, SEM images of uncontaminated coatings, details of EDS curve fitting routines, and surface EDS measurements for quantifying contaminant signal. This material is available free of charge via the Internet at http://pubs.acs.org.

AUTHOR INFORMATION

Corresponding Author

*M. P. Willis. E-mail: matthew.p.willis.civ@mail.mil. Tel: 410.436.0794.

Author Contributions

The paper was written through contributions of all authors. All authors have given approval to the final version of the paper.

Notes

The authors declare no competing financial interest.

■ ACKNOWLEDGMENTS

The authors thank Eric Lowenstein and Michael Roberts at the Defense Threat Reduction Agency (DTRA) for funding this work under contract BO09MSB317. The authors thank John Escarsega of the Army Research Laboratory and Alicia Farrell of Dynamic Science, Inc. for helpful discussions and for preparing the coating samples. The authors thank Brian Luthardt of Leidos for testing support.

■ ABBREVIATIONS

APC, Advanced Performance Coating
APG, Aberdeen Proving Ground
ARL, Army Research Laboratory
CARC, chemical agent resistant coating
CEES, 2-chloroethyl ethyl sulfide
CWA, chemical warfare agents
DMMP, dimethyl methylphosphonate
EDS, energy dispersive spectroscopy
HD, distilled mustard
SEM, scanning electron microscopy

■ REFERENCES

(1) Yang, X.; Li, J.; Croll, S.; Tallman, D.; Bierwagen, G. Degradation of Low Gloss Polyurethane Aircraft Coatings under UV and Prohesion Alternating Exposures. *Polym. Degrad. Stab.* **2003**, *80*, 51−58.
(2) Natarajan, S.; Sivan, V.; Tennyson, P.; Kiran, V. Protective Coatings on Magnesium and Its Alloys: A Critical Review. *Corros. Prev. Contr.* **2004**, *51*, 142−163.
(3) Griesser, H. Degradation of Polyurethanes in Biomedical Applications - A Review. *Polym. Degrad. Stab.* **1991**, *33*, 329−354.
(4) Miguel, M.; Tomba, J. A Comparison of Different Approaches for Depth Profiling of Films and Coatings by Confocal Raman Microscopy. *Prog. Org. Coat.* **2012**, *74*, 43−49.
(5) Gregoriou, V.; Rodman, S. Quantitative Depth Profile Analysis of Micrometer-Thick Multilayered Thin Coatings Using Step-Scan FT-IR Photoacoustic Spectroscopy. *Anal. Chem.* **2002**, *74*, 2361−2369.
(6) Frosch, T.; Chan, K.; Wong, H.; Cabral, J.; Kazarian, S. Nondestructive Three-Dimensional Analysis of Layered Polymer Structures with Chemical Imaging. *Langmuir* **2010**, *26*, 19027−19032.
(7) Davis, E.; Minelli, M.; Baschetti, M.; Elabd, Y. Non-Fickian Diffusion of Water in Polylactide. *Ind. Eng. Chem. Res.* **2013**, *52*, 8664−8673.
(8) Adamsons, K. Chemical Surface Characterization and Depth Profiling of Automotive Coating Systems. *Prog. Polym. Sci.* **2000**, *25*, 1363−1409.
(9) Kaszowska, Z.; Malek, K.; Panczyk, M.; Mikolajska, A. A Joint Application of ATR-FTIR and SEM Imaging with High Spatial Resolution: Identification and Distribution of Painting Materials and Their Degradation Products in Paint Cross Sections. *Vib. Spectrosc.* **2013**, *65*, 1−11.
(10) Kabre, J.; Lesuer, R. Modeling Diffusion of Tin into the Mesoporous Titanium Dioxide Layer of a Dye-Sensitized Solar Cell Photoanode. *J. Phys. Chem. C* **2012**, *116*, 18327−18333.
(11) Schwope, A. D.; Klein, J. M.; Sidman, K. R.; Reid, R. C. Sorption-Desorption Phenomena of Chemicals from Polymer (Paint) Films. *J. Hazard. Mater.* **1986**, *13*, 353−367.
(12) Willis, M. P.; Gordon, W. O.; Lalain, T. A.; Mantooth, B. A. Characterization of Chemical Agent Transport in Paints. *J. Hazard. Mater.* **2013**, *260*, 907−913.
(13) Notthoff, C.; Winterer, M.; Beckel, A.; Geller, M.; Heindl, J. Spatial High Resolution Energy Dispersive X-Ray Spectroscopy on Thin Lamellas. *Ultramicroscopy* **2013**, *129*, 30−35.
(14) George, S. C.; Thomas, S. Transport Phenomena through Polymeric Systems. *Prog. Polym. Sci.* **2001**, *26*, 985−1017.